





# Post-analysis of OSM-GAN Spatial Change Detection

Lasith Niroshan<sup>(✉)</sup>  and James D. Carswell 

Technological University Dublin, Dublin, Ireland

D19126805@mytudublin.ie, james.carswell@TUDublin.ie

**Abstract.** Keeping crowdsourced maps up-to-date is important for a wide range of location-based applications (route planning, urban planning, navigation, tourism, etc.). We propose a novel map updating mechanism that combines the latest freely available remote sensing data with the current state of online vector map data to train a Deep Learning (DL) neural network. It uses a Generative Adversarial Network (GAN) to perform image-to-image translation, followed by segmentation and raster-vector comparison processes to identify changes to map features (e.g. buildings, roads, etc.) when compared to existing map data. This paper evaluates various GAN models trained with sixteen different datasets designed for use by our change detection/map updating procedure. Each GAN model is evaluated quantitatively and qualitatively to select the most accurate DL model for use in future spatial change detection applications.

**Keywords:** Generative Adversarial Networks · OpenStreetMap · Remote sensing · Spatial change detection

## 1 Introduction

Conventional (manual) crowdsourced map updating procedures utilise remote sensing imagery as a background layer to guide mappers as they manually digitise objects (e.g. buildings, roads, etc.). For example, OpenStreetMap (OSM) allows for the use of multiple satellite image sources when updating their maps [1]. However, to detect changes in satellite imagery *automatically* when comparing to the latest versions of online vector maps is an important next step for many GIScience related problems, including mapping.

Previously, we introduced our methodology for detecting changes (both constructions and destructions) between vector maps and raster images [2]. Consequently, a series of experiments was conducted to evaluate the accuracy of this OSM-GAN procedure. This paper reports on these experiments and other related outcomes of OSM-GAN predictions with various datasets.

Specifically, this study evaluates the prediction accuracy of various OSM-GAN models on several spatial datasets to select the best change detection model for use in further map updating operations. Two different raster and vector data sources were tested: 8-bit (panchromatic) and 24-bit (RGB) raster image data with spatial resolution 15 cm/pixel and 30 cm/pixel [5] and; OpenStreetMap (OSM) vector map data plus Ordnance Survey

Ireland<sup>1</sup> (OSi) building footprint data of Dublin city centre were also used in conjunction with the raster data mentioned above.

## 1.1 Data Sources

### Raster Data

Raster satellite image data was used to train the OSM-GAN models for detecting any changes to the map in a given Area of Interest (AoI). First, a satellite image dataset was created using freely available Google Earth satellite images discovered online using customised data *crawlers* that considers both spatial resolution (15 cm and 30 cm) and AoI. Second, a 25 cm resolution aerial orthophoto dataset of Dublin area registered to the Irish Transverse Mercator (ITM) coordinate system was acquired from OSi with an academic research license.

These TIFF (Tagged Image File Format) orthophotos needed to be pre-processed before inputting to the deep neural network – e.g., resampled to 30 cm pixels, co-registered, tiled, and served from QGIS<sup>2</sup>. Figure 1 shows the qualitative differences between both data sources (Google Earth and OSi). Note how some buildings currently visible in the Google Earth imagery are not present in the OSi orthophotos as they have since been demolished in preparation for constructing the new TU Dublin campus.



**Fig. 1.** Comparison of Google Earth satellite images (first row) and OSi aerial ortho images (second row) of the same AoI around Grangegorman, Dublin. The displayed resolution for both is 30 cm/pixel. The Google Earth images appear more vivid, the OSi images can be obtained at a higher resolution.

### Vector Data

OSM vector data was the primary map data source checked for changes in this study. As OSi building footprint (vector) data is produced by Ireland’s National Mapping Agency, it was used as ground truth for model training and prediction purposes. The OSM vector

<sup>1</sup> <https://osi.ie/>.

<sup>2</sup> [https://docs.qgis.org/3.16/en/docs/user\\_manual/preamble/preamble.html](https://docs.qgis.org/3.16/en/docs/user_manual/preamble/preamble.html).

data was downloaded using their *Overpass* API [3] by first parsing the minimum bounding rectangle (MBR) of a user generated AoI. The OSi building footprints were provided in DWG (AutoCAD) format. A series of operations converted the DWG formatted data into *GeoJSON* format to be compatible with further processing steps. Table 1 gives a summary of both the OSM and OSi building footprint datasets.

**Table 1.** Details of the two vector datasets.

	OSM dataset	OSi dataset
Area of interests	Selective areas around Grangegorman, Dublin	53.3514000, -6.2892000, 53.3596000, -6.2730000
Number of objects	15,000+	3036
Spatial reference system	EPSG:3857 (Spherical Mercator projection)	Irish Transverse Mercator (ITM)
License	Open Database License (ODbL)	OSi License
Data format	JSON, GeoJSON	DWG

## 1.2 The Kay Supercomputer

The Irish Centre for High-End Computing (ICHEC) allows institutional users (e.g. academic researchers) access to its super computing infrastructure, named *Kay* [4]. *Kay* is comprised of five sub-components: Cluster, GPU, Phi, High Memory, and Service and Storage. Specifically, for experiments in this study, the GPU service was utilised.

The GPU service is a partition of 16 nodes where each node has  $2 \times 20$ -core 2.4 GHz Intel Xeon Gold 6148 (Skylake) processors, 192 GiB of RAM, a 400 GiB local SSD for scratch space and a 100 Gbit Omni-Path network adaptor. Two NVIDIA Tesla V100 16 GB PCIe (Volta architecture) GPUs are integrated on each node. Each GPU has 5,120 CUDA cores and 640 Tensor Cores. In order to reduce training times, this study tested the *Kay* Supercomputer with various parameter settings [4]. As such, overall training times per model reduced from a few days spent training on a high-end “gamer spec” laptop, to just a few hours on *Kay*.

## 2 Related Work

Spatial change detection is a well-researched area in both the GIScience and computer vision domains. Historically, many different image processing techniques, including Markov Random Field [6] and Principal Component Analysis [7], were used to perform spatial change detection operations. More recently, artificial neural network-based techniques have been introduced to address various limitations of more traditional approaches (e.g. to overcome low performance, low segmentation accuracy, higher time complexity, etc.).

Now, common solutions to this problem rely on applying Machine Learning (ML) techniques such as *U-Net* [8], *SegNet* [9, 10], *Mask R-CNN* [11], and *Pix2Pix* among others [12, 13]. These approaches follow the encoder-decoder architecture to perform *image segmentation*, a critical step in any change detection process. In particular to GIS, image segmentation attempts to isolate various entities in the environment visible in aerial imagery. For example, entities such as buildings [14–16], road networks [17–24], and land-use classifications [25–28].

With the emergence of Generative Adversarial Networks (GANs), image segmentation procedures have been redefined as image-to-image *translation*. GANs are a ML technique of training a generative neural network model by representing the task as a supervised learning problem with two sub-models: a *generator* that learns to generate new examples; and a *discriminator* that tries to classify these generated examples as either *real* or *fake* (generated) [29]. Several studies have proposed GAN-based solutions for various spatial change detection problems, such as generating heat-maps of possible changes [30], seasonal change detection [31], and image classifications [32].

## 2.1 OSM-GAN for Spatial Change Detection

The OSM-GAN approach presented in this paper suggests a change detection methodology that employs spatial imagery (satellite images) and OSM vector map data [2] to train its models. The deep learning model should be accurate enough to detect image objects (e.g. buildings) to predict any change detection outcomes to these map features. Technically, the OSM-GAN model needs to perform a satellite image to feature-map translation with a high confidence level [2]. This paper proposes a methodology to evaluate various GAN models (trained with different datasets to perform satellite image to feature-map translation) to detect spatial changes accurately.

Producing our OSM-GAN model begins with the data *crawling* process. Freely available raster and vector data sources are crawled (mined) and saved in local directory structures ready for further processing. Geo-referenced satellite images are merged to construct the left half of the training sample, and OSM vectors are merged into a binary (black & white) single image to create the right half of the training sample. This process results in a single  $600 \times 300$  pixel sized training sample as shown in Fig. 2.



**Fig. 2.** One sample of the OSM-GAN training dataset. The left side illustrates the satellite image component, and the right side shows the corresponding *feature-map*.

An object-density based data filtering mechanism is used to remove false-negative data samples from the training dataset [2]. The filtered dataset is then split into a 3:2 ratio of *training:validation* sets of data. Finally, these datasets were fed into the training algorithm on the Kay supercomputer to generate the resulting OSM-GAN model.

To initiate the change detection process, a *feature-map* (binary image that represents particular map features (e.g. buildings) as white blobs) needs to be predicted for a particular satellite image using the OSM-GAN model generated previously. Then the predicted feature-map is segmented into separate objects and compared to current OSM vector data using an Overlap Score Matrix (percent overlap of a feature-map object and its OSM vector footprint). Finally, any detected changes are post-processed to compose OSM-acceptable *changesets*. Figure 3 illustrates the overall workflow for spatial change detection based on OSM-GAN.

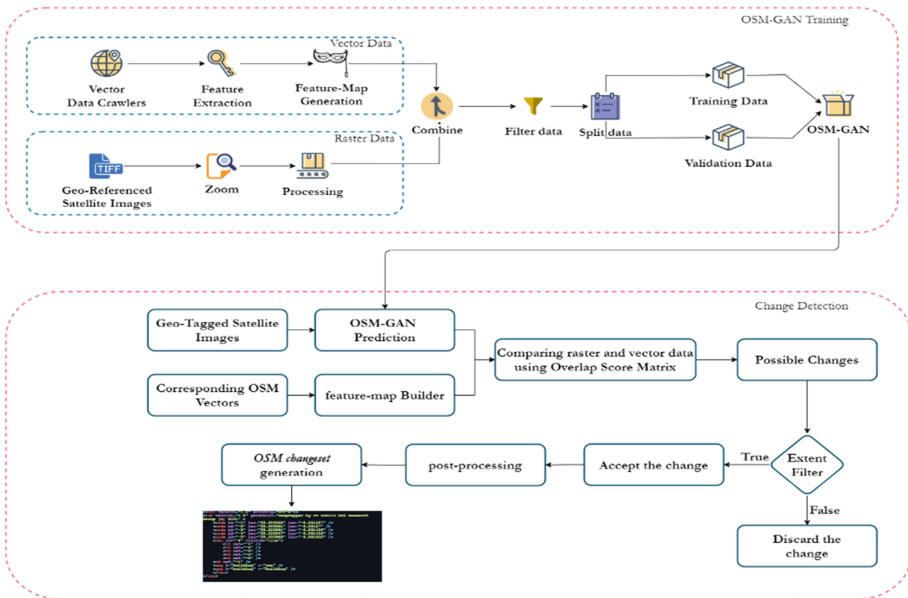


Fig. 3. System architecture of proposed OSM-GAN methodology for spatial change detection.

### 3 Experiments and Results

For this study, a series of experiments were conducted to evaluate the accuracy of OSM-GAN models qualitatively and quantitatively. Sixteen OSM-GAN models were trained with different datasets. A combination of two different spatial resolutions (15 cm and 30 cm) with two different types of images (panchromatic and RGB) were used to create the raster image segment (left half of the training sample). OSM and OSi vector data were used to create the right half of the training sample (Fig. 2). For instance, the

*Google\_OSi\_8bit\_z19* dataset was created from panchromatic (8-bit) Google Earth satellite images with 30 cm/pixel and OSi vectors. After the training process, the final model is named the same as the name of the dataset used to create it.

### 3.1 Modelling OSM-GAN with OSi Data

OSi raster (orthophotos resampled to 30 cm and 15 cm pixels to match the satellite data) and vector building footprint data was used in this experiment. Four datasets with different spatial resolutions and bit-depth were created from the above-mentioned sources. These datasets were smaller than the OSM datasets since the data provided by OSi was of a limited area of Dublin city centre only. Table 2 summarises the two datasets produced for this experiment.

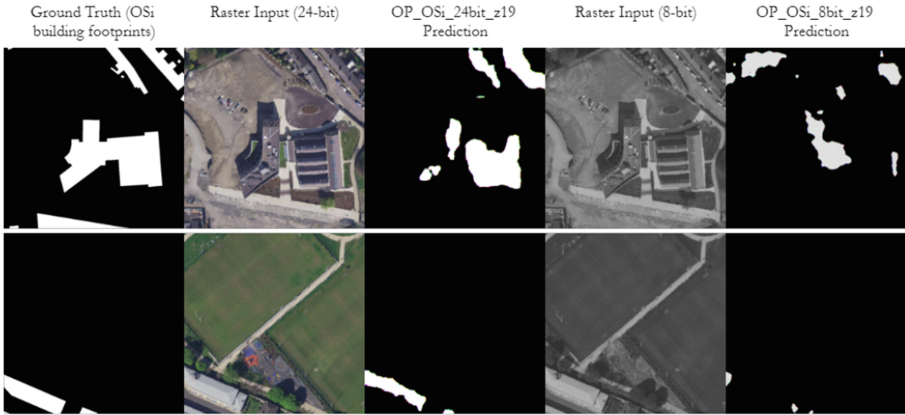
**Table 2.** Details of datasets used in OSi-OSi experiment

	Dataset 1	Dataset 2	Dataset 3	Dataset 4
Raster source	OSi Orthophotos			
Vector source	OSi building footprints			
Resolution	30 cm ( <i>z19</i> )		15 cm ( <i>z20</i> )	
Bit-depth	8-bit	24-bit	8-bit	24-bit
Number of samples	581	581	1949	1949
Model ID	OP_OSi_8bit_z19	OP_OSi_24bit_z19	OP_OSi_8bit_z20	OP_OSi_24bit_z20

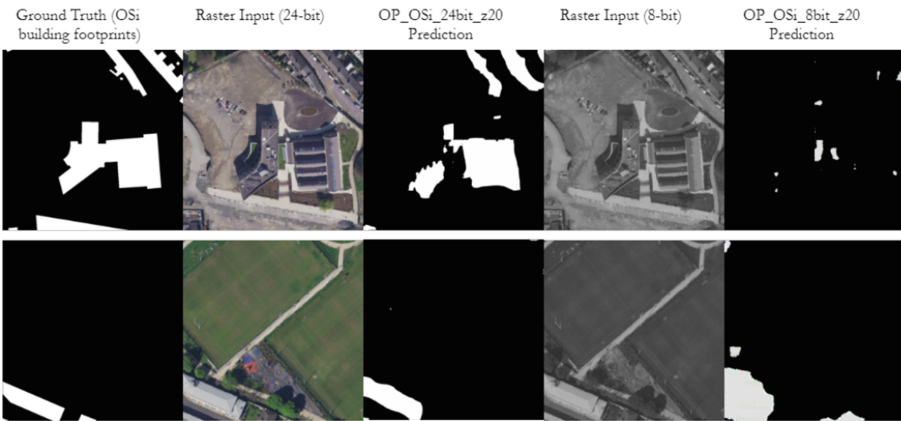
Upon completion of the training process, each model was evaluated on a new dataset within the same AoI. These results were qualitatively and quantitatively evaluated, and Accuracy, Recall, Precision and F1 score measurements were calculated for each model (Table 3). The model trained with 30 cm/pixel resolution RGB images can be considered more accurate than the other three models.

**Table 3.** Quantitative evaluation of the model trained with OSi Orthophoto and OSi vector data

Model ID	Accuracy	Precision	Recall	F1 score
OP_OSi_8bit_z19	68.3%	82.0%	45.9%	58.8%
<b>OP_OSi_24bit_z19</b>	86.8%	84.6%	82.1%	83.3%
OP_OSi_8bit_z20	65.3%	70.9%	40.6%	51.6%
OP_OSi_24bit_z20	84.0%	85.0%	72.4%	78.2%



a) Comparison of predictions from model trained with 30cm/pixel dataset



b) Comparison of predictions from model trained with 15cm/pixel dataset

**Fig. 4.** Predictions of OSM-GAN model trained with OSi Orthophotos and building footprints.

Figure 4 qualitatively compares the outcomes of the above-listed OSM-GAN model predictions. It can be seen in Fig. 4a that the OP\_OSi\_24bit\_z19 model gives comparatively more accurate results, demonstrating the importance of a qualitative analysis of testing. For example, the OP\_OSi\_8bit\_z20 model predicted a large building that could be identified as an “extension” to existing OSi vector data by the subsequent change detection process.

### 3.2 Modelling OSM-GAN with OSi-OSM Data

The second experiment was designed to investigate the consistency/coherence between OSi Orthophotos and OSM vectors. Apart from a difference in the spatial reference system used, it was observed that current OSM vectors of the test area are outdated. Therefore, many data samples were filtered out in the data filtering phase. Table 4 summarises the generated datasets using OSi Orthophoto images and OSM vectors.

**Table 4.** Details of datasets employed in OSi-OSM experiments.

	Dataset 1	Dataset 2	Dataset 3	Dataset 4
Raster source	OSi orthophotos			
Vector source	OSM building footprints			
Resolution	30 cm ( <i>z19</i> )		15 cm ( <i>z20</i> )	
Bit-depth	8-bit	24-bit	8-bit	24-bit
Number of samples	641	641	1993	1993
Model ID	OP_OSM_8bit_z19	OP_OSM_24bit_z19	OP_OSM_8bit_z20	OP_OSM_24bit_z20

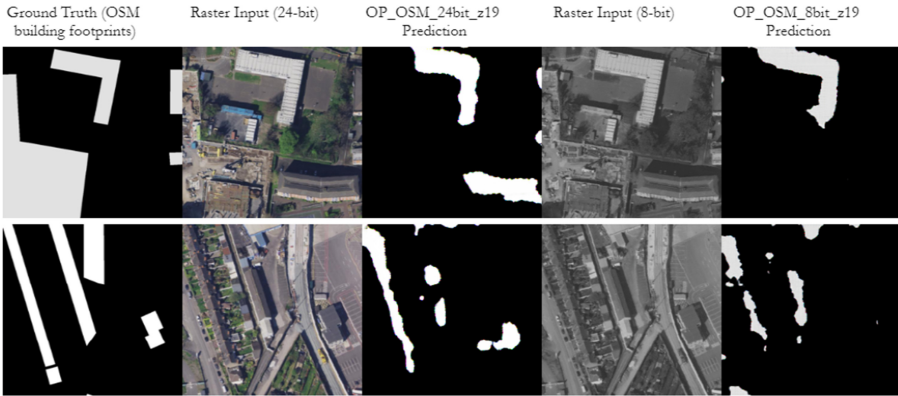
A quantitative analysis of the testing results is listed in Table 5. In this case, the model trained with a 30 cm (*z19*) 8-bit dataset showed the highest accuracy, while the first experiment produced a model trained on RGB images as the most accurate; in both cases with the same resolution.

**Table 5.** Quantitative results of the OSi-OSM experiment.

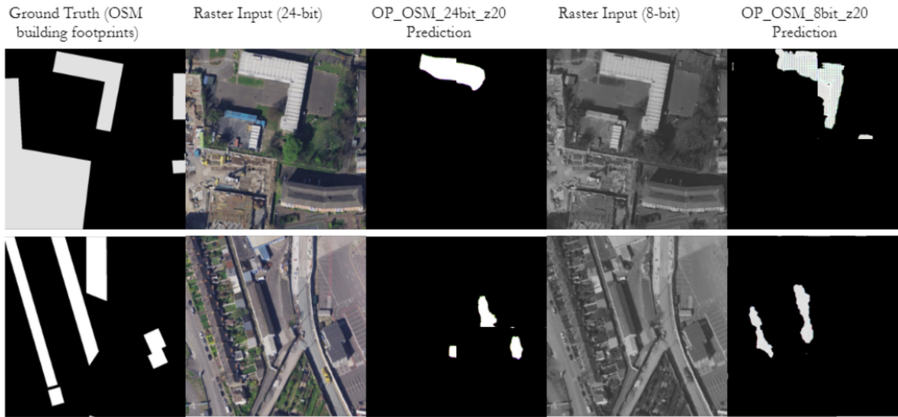
Model ID	Accuracy	Precision	Recall	F1 score
<b><i>OP_OSM_8bit_z19</i></b>	76.4%	58.7%	67.3%	62.71%
OP_OSM_24bit_z19	72.1%	63.4%	70.8%	66.90%
OP_OSM_8bit_z20	50.6%	52.0%	55.4%	53.65%
OP_OSM_24bit_z20	20.2%	47.3%	61.9%	53.62%

Figure 5 illustrates the qualitative comparisons of the models in Table 5. Since visual comparisons show only two random instances taken from the test dataset, the visual results perhaps do not support well the quantitative measurements obtained above. However, to improve the change detection workflow, the results should be accurate both quantitatively and qualitatively.





a) Comparison of predictions of the model trained with 30cm/pixel dataset



b) Comparison of predictions of the model trained with 15cm/pixel dataset

**Fig. 5.** Qualitative analysis of predictions from the model trained with OSi Orthophotos and OSM building footprints.

### 3.3 Modelling OSM-GAN with Google-OSi Data

Models with Google Earth satellite images and OSi building footprints were trained in a third experiment. Four datasets were created using different spatial resolutions and bit-depths. A relatively small AoI fitting OSi boundary constraints was applied to the Google Earth image crawler to collect the relevant satellite images or the area. Table 6 summarises the details about these datasets.

**Table 6.** Details of the datasets that used in the Google-OSi experiments.

	Dataset 1	Dataset 2	Dataset 3	Dataset 4
Raster source	Google earth satellite images			
Vector source	OSi building footprints			
Resolution	30 cm ( <i>z19</i> )		15 cm ( <i>z20</i> )	
Bit-depth	8-bit	24-bit	8-bit	24-bit
Number of samples	644	644	2110	2110
Model ID	Google_OSi_8bit_z19	Google_OSi_24bit_z19	Google_OSi_8bit_z20	Google_OSi_24bit_z20

Table 7 lists the quantitative measurements calculated for the trained models. A model trained with 15 cm RGB images scored better quantitative results than the other three models. After comparing to previous experiments (OSi-OSi and OSi-OSM), the model trained with higher resolution images is quantitatively more accurate.

**Table 7.** Quantitative results obtained from experiments conducted with Google-OSi datasets

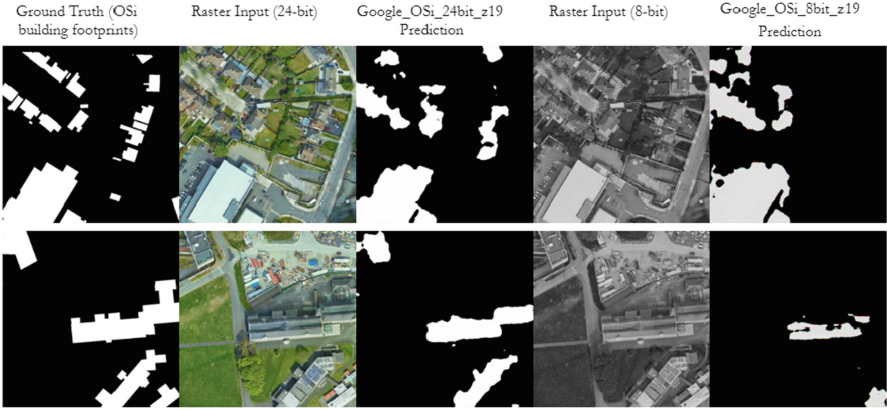
Model ID	Accuracy	Precision	Recall	F1 score
Google_OSi_8bit_z19	66.7%	48.7%	30.6%	37.6%
Google_OSi_24bit_z19	83.0%	68.0%	71.2%	69.56%
Google_OSi_8bit_z20	71.9%	66.6%	62.1%	64.2%
<b>Google_OSi_24bit_z20</b>	85.4%	75.80%	81.10%	78.36%

Figure 6 shows a qualitative comparison of some prediction samples. The predictive results of the Google\_OSi\_24bit\_z20 model (Fig. 6b) agree with the above quantitative results. The predicted polygons can be used in the subsequent change detection process since they are allied to ground truth polygons.

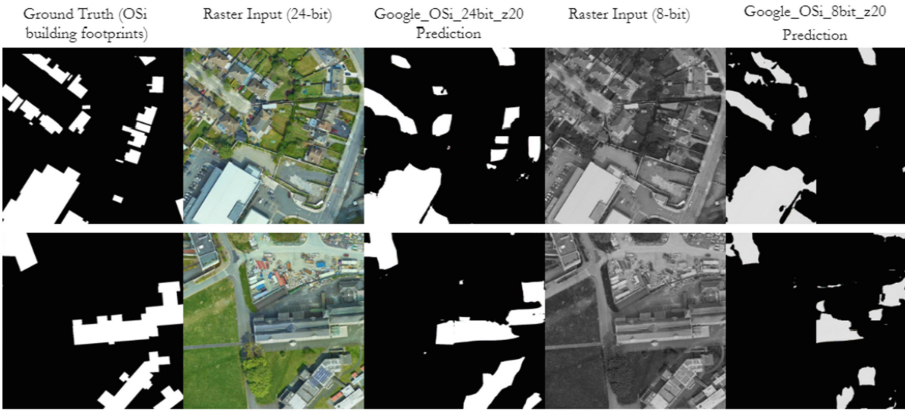
### 3.4 Modelling OSM-GAN with Google-OSM Data

Finally, yet importantly, Google Earth satellite images and OSM vectors were combined to perform another training phase. Since both data resources are free and unlimited, a wider AoI was chosen and crawled to create the following datasets.

The above-listed datasets were used to train four OSM-GAN models. These models were then evaluated using the same accuracy measurements such as Accuracy, Recall, Precision, and F1 Score (Table 9). The model trained with 30 cm RGB Google Earth satellite images and OSM vector footprints performed better. Significantly, this is the most accurate OSM-GAN model obtained when compared to all the models evaluated in the four experiments.



a) Comparison of predictions of the model trained with 30cm/pixel dataset



b) Comparison of predictions of the model trained with 15cm/pixel dataset

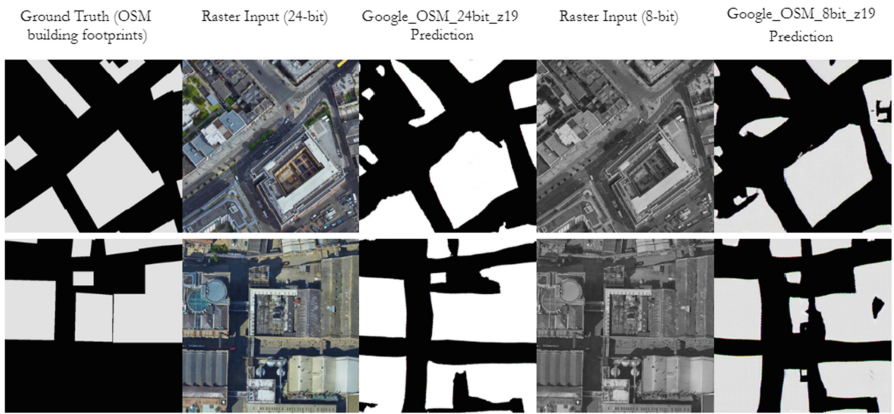
**Fig. 6.** Predictions of models trained with Google Earth satellite images and OSi buildings.

**Table 8.** Details of datasets used in Google-OSM experiment.

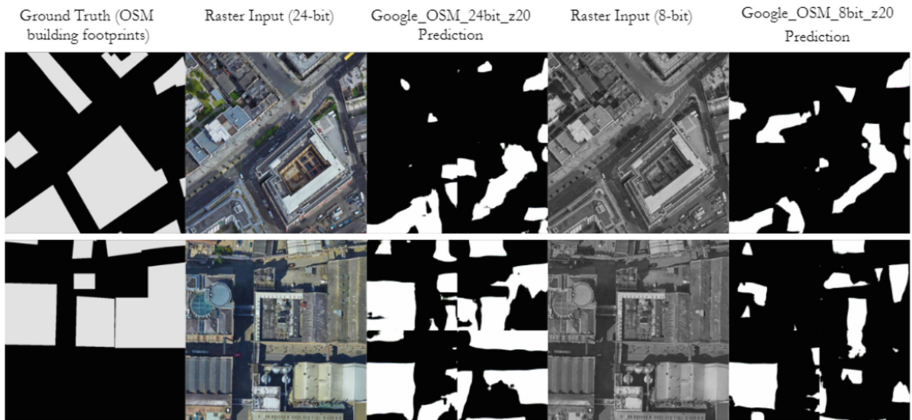
	Dataset 1	Dataset 2	Dataset 3	Dataset 4
Raster source	Google earth satellite images			
Vector source	OSM building footprints			
Resolution	30 cm (z19)		15 cm (z20)	
Bit-depth	8-bit	24-bit	8-bit	24-bit
Number of samples	644	644	2110	2110
Model ID	Google_OSM_8bit_z19	Google_OSM_24bit_z19	Google_OSM_8bit_z20	Google_OSM_24bit_z20

**Table 9.** Quantitative measurements obtained from the final experiment.

Model ID	Accuracy	Precision	Recall	F1 score
Google_OSM_8bit_z19	86.7%	59.3%	78.1%	67.4%
<b>Google_OSM_24bit_z19</b>	88.4%	62.0%	80.5%	70.0%
Google_OSM_8bit_z20	35.2%	45.8%	61.3%	52.4%
Google_OSM_24bit_z20	68.0%	50.4%	53.7%	52.0%



a) Comparison of predictions of the model trained with 30cm/pixel dataset



b) Comparison of predictions of the model trained with 15cm/pixel dataset

**Fig. 7.** Qualitative comparisons of models trained with Google Earth satellite images and OSM building footprints.

Figure 7 qualitatively compares the prediction results of models trained with Google Earth satellite images and OSM building footprints. In this case, the prediction results of *Google\_OSM\_24bit\_z19* shows the best qualitative test result, agreeing with the quantitative results above. Comparing all 16 models tested, the results of model *Google\_OSM\_24bit\_z19* suggests to train 30 cm Google Earth satellite images with OSM vector data to obtain the most accurate OSM-GAN models for change detection.

## 4 Conclusions

This paper presented sixteen different OSM-GAN based experiments with a quantitative analysis of each model produced, as well some qualitative observations. It evaluated different OSM-GAN models against different raster and vector data sources. Each dataset offers its own benefits and limitations and the qualitative results motivated continued training with larger area datasets.

The study concludes that the vector footprint generated by OSM-GAN image-to-image translation could be extended to spatial change detection procedures. Experiments show that model training with larger datasets (i.e. datasets built from Google Earth satellite images and OSM building footprints) yielded more accurate feature-map predictions.

Since the proposed spatial change detection methodology is highly based on OSM-GAN model accuracy, the model should be as accurate as possible to translate a satellite image to its corresponding feature-map. The final experiment reveals that training on larger sets of geographically similar areas could be a solution to generating more accurate OSM-GAN models. In other words, models trained with Dublin data should not be used for mapping Paris, for example. The model trained with Google Earth satellite images (24-bit, 30 cm/pixel) and OSM building footprints scored the highest accuracy (88.4%) among all the experiments. Moreover, the predictions of the *Google\_OSM\_24bit\_z19* model can also be observed qualitatively as more accurate than the other model predictions.

The ultimate objective of this research is to build an end-to-end workflow to update crowdsourced maps automatically with the use of freely available data (satellite images, vector footprints) and Artificial Intelligence (AI) techniques. Automated map update success ultimately depends on the accuracy of the ML change detection process since correctly identifying spatial changes in the map is an initial key step in this process. Compared to contemporary approaches for automatically detecting spatial changes, the proposed OSM-GAN approach offers an appropriate mechanism to follow.

As a next step, a new OSM-GAN model will be trained on the original 25 cm Dublin orthophotos with a larger AoI to potentially produce even more accurate feature-map results. The training process will utilise a *Transfer Learning* approach and so begins by initiating the process using the *Google\_OSM\_24bit\_z19* model parameters as the base input model. In order to evaluate the performance and accuracy of OSM-GAN against other spatial change detection models in the literature, a new test phase will also be carried out on the *crowdAI Mapping Challenge* dataset<sup>3</sup> in future work.

<sup>3</sup> <https://www.crowdai.org/challenges/mapping-challenge>.

**Acknowledgements.** The authors wish to thank all contributors involved with the OpenStreetMap project. This research is funded by Technological University Dublin College of Arts and Tourism, SEED FUNDING INITIATIVE 2019–2020. The authors wish to acknowledge the Irish Centre for High-End Computing (ICHEC) for the provision of computational facilities and support. We also gratefully acknowledge Ordnance Survey Ireland for providing both raster and vector data for the experiments.

## References

1. OpenStreetMap. <https://www.openstreetmap.org>. Accessed 22 Sept 2021
2. Niroschan, L., Carswell, J.D.: OSM-GAN: using generative adversarial networks for detecting change in high-resolution spatial images. In: 5th International Conference on Geoinformatics and Data Analysis (ICGDA 2022), Paris, France, January 2022, Springer Lecture Notes on Data Engineering and Communications Technologies (2022)
3. Overpass API. [https://wiki.openstreetmap.org/wiki/Overpass\\_API](https://wiki.openstreetmap.org/wiki/Overpass_API). Accessed 29 Oct 2021
4. Kay. <https://www.ichec.ie/about/infrastructure/kay>. Accessed 15 Sept 2021
5. What is bit depth? <https://etc.usf.edu/techease/win/images/what-is-bit-depth/>. Accessed 15 Oct 2021
6. Gong, M., Su, L., Jia, M., Chen, W.: Fuzzy clustering with a modified MRF energy function for change detection in synthetic aperture radar images. *IEEE Trans. Fuzzy Syst.* **22**(1), 98–109 (2013)
7. Yousif, O., Ban, Y.: Improving urban change detection from multitemporal SAR images using PCA-NLM. *IEEE Trans. Geosci. Remote Sens.* **51**(4), 2032–2041 (2013)
8. Ronneberger, O., Fischer, P., Brox, T.: U-Net: convolutional networks for biomedical image segmentation. In: Proceedings of the International Conference on Medical Image Computing and Computer-Assisted Intervention, Munich, Germany, 5–9 October 2015, pp. 234–241 (2015)
9. Badrinarayanan, V., Kendall, A., Cipolla, R.: SegNet: a deep convolutional encoder-decoder architecture for image segmentation. *IEEE Trans. Pattern Anal. Mach. Intell.* **39**, 2481–2495 (2017)
10. SegNet. <https://mi.eng.cam.ac.uk/projects/segnet/>. Accessed 20 Sept 2021
11. He, K., Gkioxari, G., Dollár, P., Girshick, R.: Mask R-CNN. In: Proceedings of the IEEE International Conference on Computer Vision, Venice, Italy, 22–29 October 2017, pp. 2961–2969 (2017)
12. Isola, P., Zhu, J.Y., Zhou, T., Efros, A.A.: Image-to-image translation with conditional adversarial networks. In: Proceedings of the 2017 IEEE Conference on Computer Vision and Pattern Recognition (CVPR), Honolulu, HI, USA, 21–26 July 2017, pp. 5967–5976 (2017)
13. Image-to-Image Translation with Conditional Adversarial Networks. <https://phillipi.github.io/pix2pix/>. Accessed 20 Sept 2021
14. Tiecke, T.G., et al.: Mapping the World Population One Building at a Time. arXiv 2017, arXiv:cs/1712.05839
15. Iglovikov, V., Seferbekov, S.S., Buslaev, A., Shvets, A.: TeraNetV2: fully convolutional network for instance segmentation. In: Proceedings of the Conference on Computer Vision and Pattern Recognition Workshops (CVPRW), Salt Lake City, UT, USA, 18–22 June 2018, vol. 233, p. 237 (2018)
16. Microsoft/USBuildingFootprints. <https://github.com/microsoft/USBuildingFootprints>. Accessed 20 Sept 2021

17. Zhou, L., Zhang, C., Wu, M.: D-LinkNet: LinkNet with pretrained encoder and dilated convolution for high resolution satellite imagery road extraction. In: Proceedings of the 2018 IEEE/CVF Conference on Computer Vision and Pattern Recognition Workshops (CVPRW), Salt Lake City, UT, USA, 18–22 June 2018, pp. 192–1924 (2018)
18. Oehmcke, S., Thrysoe, C., Borgstad, A., Salles, M.A.V., Brandt, M., Gieseke, F.: Detecting hardly visible roads in low-resolution satellite time series data. arXiv 2019. [arXiv:1912.05026](https://arxiv.org/abs/1912.05026)
19. Buslaev, A., Seferbekov, S.S., Igloukov, V., Shvets, A.: Fully convolutional network for automatic road extraction from satellite imagery. In: Proceedings of the Conference on Computer Vision and Pattern Recognition Workshops (CVPRW), Salt Lake Cit, UT, USA, 18–22 June 2018, pp. 207–210 (2018)
20. Xia, W., Zhang, Y.Z., Liu, J., Luo, L., Yang, K.: Road extraction from high resolution image with deep convolution network—a case study of GF-2 image. In: Multidisciplinary Digital Publishing Institute Proceedings, MDPI: Basel, Switzerland, vol. 2, p. 325 (2018)
21. Wu, S., Du, C., Chen, H., Xu, Y., Guo, N., Jing, N.: Road extraction from very high resolution images using weakly labeled OpenStreetMap centerline. ISPRS Int. J. Geo-Inf. **8**, 478 (2019)
22. Xia, W., Zhong, N., Geng, D., Luo, L.: A weakly supervised road extraction approach via deep convolutional nets based image segmentation. In: Proceedings of the 2017 International Workshop on Remote Sensing with Intelligent Processing (RSIP), Shanghai, China, 19–21 May 2017, pp. 1–5 (2017)
23. Sun, T., Di, Z., Che, P., Liu, C., Wang, Y.: Leveraging crowdsourced GPS data for road extraction from aerial imagery. In: Proceedings of the IEEE Conference on Computer Vision and Pattern Recognition, Long Beach, CA, USA, 16–20 June 2019, pp. 7509–7518 (2019)
24. Ruan, S., et al.: Learning to generate maps from trajectories. In: Proceedings of the AAAI Conference on Artificial Intelligence, New York, NY, USA, 7–8 February 2020
25. Albert, A., Kaur, J., Gonzalez, M.C.: Using convolutional networks and satellite imagery to identify patterns in urban environments at a large scale. In: Proceedings of the 23rd ACM SIGKDD International Conference on Knowledge Discovery and Data Mining, Halifax, NS, Canada, 13–17 August 2017, pp. 1357–1366 (2017)
26. Rakhlin, A., Davydow, A., Nikolenko, S.I.: Land cover classification from satellite imagery with U-Net and Lovasz-Softmax loss. In: Proceedings of the Conference on Computer Vision and Pattern Recognition Workshops (CVPRW), Salt Lake City, UT, USA, 18–22 June 2018, pp. 262–266 (2018)
27. Cao, R., et al.: Integrating aerial and street view images for urban land use classification. Remote Sens. **10**, 1553 (2018)
28. Kuo, T.S., Tseng, K.S., Yan, J.W., Liu, Y.C., Wang, Y.C.F.: Deep aggregation net for land cover classification. In: Proceedings of the Conference on Computer Vision and Pattern Recognition Workshops (CVPRW), Salt Lake Cit, UT, USA, 18–22 June 2018, pp. 252–256 (2018)
29. Schmidhuber, J.: Unsupervised minimax: adversarial curiosity, generative adversarial networks, and predictability minimization. arXiv 2019, arXiv:cs/1906.04493
30. Albrecht, C.M., et al.: Change detection from remote sensing to guide OpenStreetMap labeling. ISPRS Int. J. Geo Inf. **9**(7), 427 (2020)
31. Lebedev, M.A., Vizilter, Y.V., Vygolov, O.V., Knyaz, V.A., Rubis, A.Y.: Change detection in remote sensing images using conditional adversarial networks. International Archives of the Photogrammetry, Remote Sensing & Spatial Information Sciences, **42**(2) (2018)
32. Papadomanolaki, M., Verma, S., Vakalopoulou, M., Gupta, S., Karantzas, K.: Detecting urban changes with recurrent neural networks from multi-temporal Sentinel-2 data. In: IGARSS 2019–2019 IEEE International Geoscience and Remote Sensing Symposium, pp. 214–217. IEEE, July 2019